The Astrophysical Journal Letters, 746:L20 (5pp), 2012 February 20 doi:10.1088/2041-8205/746/2/L20

AN EXTREME X-RAY DISK WIND IN THE BLACK HOLE CANDIDATE IGR J17091−3624

A. L. King[1], J. M. Miller[1], J. Raymond[2], A. C. Fabian[3], C. S. Reynolds[4], T. R. Kallman[5], D. Maitra[1], E. M. Cackett[3,6], and M. P. Rupen[7]
[1] Department of Astronomy, University of Michigan, 500 Church Street, Ann Arbor, MI 48109-1042, USA; ashking@umich.edu
[2] Smithsonian Astrophysical Observatory, 60 Garden Street, Cambridge, MA 02138, USA
[3] Institute of Astronomy, University of Cambridge, Madingley Road, Cambridge, CB3 OHA, UK
[4] Department of Astronomy, University of Maryland, College Park, MD 20742, USA
[5] Laboratory for High Energy Astrophysics, NASA Goddard Space Flight Center, Code 662, Greenbelt, MD 20771, USA
[6] Department of Physics and Astronomy, Wayne State University, Detroit, MI 48201, USA
[7] National Radio Astronomy Observatory, Socorro, NM 87801, USA
Received 2011 December 15; accepted 2012 January 9; published 2012 January 31

ABSTRACT

Chandra spectroscopy of transient stellar-mass black holes in outburst has clearly revealed accretion disk winds in soft, disk-dominated states, in apparent anti-correlation with relativistic jets in low/hard states. These disk winds are observed to be highly ionized, dense, and to have typical velocities of ∼1000 km s^{-1} or less projected along our line of sight. Here, we present an analysis of two *Chandra* High Energy Transmission Grating spectra of the Galactic black hole candidate IGR J17091−3624 and contemporaneous Expanded Very Large Array (EVLA) radio observations, obtained in 2011. The second *Chandra* observation reveals an absorption line at 6.91 ± 0.01 keV; associating this line with He-like Fe XXV requires a blueshift of 9300^{+500}_{-400} km s^{-1} (0.03*c*, or the escape velocity at 1000 $R_{\rm Schw}$). This projected outflow velocity is an order of magnitude higher than has previously been observed in stellar-mass black holes, and is broadly consistent with some of the fastest winds detected in active galactic nuclei. A potential feature at 7.32 keV, if due to Fe XXVI, would imply a velocity of ∼14,600 km s^{-1} (0.05*c*), but this putative feature is marginal. Photoionization modeling suggests that the accretion disk wind in IGR J17091−3624 may originate within 43,300 Schwarzschild radii of the black hole and may be expelling more gas than it accretes. The contemporaneous EVLA observations strongly indicate that jet activity was indeed quenched at the time of our *Chandra* observations. We discuss the results in the context of disk winds, jets, and basic accretion disk physics in accreting black hole systems.

Key words: accretion, accretion disks – black hole physics – X-rays: binaries

Online-only material: color figures

1. INTRODUCTION

A detailed observational account of how black hole accretion disks drive winds and jets remains elusive, but the combination of high-resolution X-ray spectroscopy, improved radio sensitivity, and comparisons across the black hole mass scale hold great potential. The broad range in X-ray luminosity covered by transient stellar-mass black holes makes it possible to trace major changes in the accretion flow as a function of the inferred mass accretion rate; this is largely impossible in supermassive black holes. Disk winds and jets, for instance, appear to be state-dependent and mutually exclusive in sources such as H 1743−322 (Miller et al. 2006b; Blum et al. 2010), GRO J1655−40 (Miller et al. 2008; Luketic et al. 2010; Kallman et al. 2009), and GRS 1915+105 (Miller et al. 2008; Neilsen & Lee 2009). This may offer insights into why many Seyfert active galactic nuclei (AGNs), which are well known for their disk winds, are typically radio-quiet (though not necessarily devoid of jets; see King et al. 2011; Jones et al. 2011; Giroletti & Panessa 2009).

The proximity of Galactic black hole binaries (BHBs) ensures a high flux level and spectra with excellent sensitivity in the Fe K band. This is of prime importance because He-like Fe XXV and H-like Fe XXVI lines can endure in extremely hot, ionized gas (see, e.g., Bautista & Kallman 2001), and therefore trace the wind region closest to where it is launched near the black hole. Studies of some stellar-mass black hole disk winds find that the gas is too ionized, too dense, and originates too close to the black hole to be expelled by radiative pressure or by thermal pressure from Compton heating of the disk, requiring magnetic pressure (Miller et al. 2006a, 2006b; Kubota et al. 2007). Winds that may originate close to the black hole and carry high mass fluxes are also observed in AGNs (e.g., Kaspi et al. 2002; Chartas et al. 2002; King et al. 2012; Tombesi et al. 2010).

In this Letter, we present evidence of a particularly fast disk wind in the black hole candidate IGR J17091−3624. The current outburst of IGR J17091−3624 was first reported on 2011 January 28 (Krimm et al. 2011). Our observations caught IGR J17091−3624 in the high/soft state, but it is important to note that the source has also showed low/hard state episodes with flaring and apparent jet activity in radio bands (Rodriguez et al. 2011). X-ray flux variations in IGR J17091−3264 bear similarities to the microquasar GRS 1915+105 (e.g., Altamirano et al. 2011a).

2. OBSERVATION AND DATA REDUCTION

IGR J17091−3624 was first observed with *Chandra* on 2011 August 1 (ObsID 12405), starting at 06:59:16 (UT), for a total of 30 ks. The High Energy Transmission Gratings (HETG) were used to disperse the incident flux onto the Advanced CCD Imaging Spectrometer spectroscopic array (ACIS-S). To prevent photon pile-up, the ACIS-S array was operated in continuous clocking or "GRADED_CC" mode, which reduced the nominal frame time from 3.2 s to 2.85 ms. The zeroth-order flux is incident on the S3 chip, and frames from this chip can be lost from the telemetry stream if a source is very bright. We therefore used a gray window over the zeroth-order aim point; only 1 in

10 photons was telemetered within this region. For a longer discussion of this mode, please see, e.g., Miller et al. (2006b, 2008). The source was observed for a second time on 2011 October 6, starting at 11:17:02 (UT), again for a total of 30 ks. The relatively low flux observed during the first observation indicated that the ACIS-S array could be operated in the standard "timed event" imaging mode during this second observation.

Data reduction was accomplished using CIAO version 4.1 (Fruscione et al. 2006). Time-averaged first-order High Energy Grating (HEG) and Medium Energy Grating (MEG) spectra were extracted from the Level-2 event file. Redistribution matrix files (rmfs) were generated using the tool "mkgrmf"; ancillary response files (arfs) were generated using "mkgarf." The first-order HEG spectra and responses were combined using the tool "add_grating_orders." The spectra were then grouped to require a minimum of 10 counts bin^{-1}. All spectral analyses were conducted using XSPEC version 12.6.0. All errors quoted in this Letter are 1σ errors.

Nearly simultaneous radio observations were made with the Expanded Very Large Array (EVLA) at each *Chandra* pointing. The first radio epoch included a 2 hr integration at 8.4 GHz on 2011 August 2 (MJD 55776) at 1:01:04 (UT), while the second was a 2 hr integration at both 8.4 and 4.8 GHz on 2011 October 6 (MJD 55841) at 22:10:16 (UT). The flux and bandpass calibrator was 3C 286. The phase and gain calibrators were J1720−3552 and J1717−3624 for the first and second observations, respectively. The data are reduced using CASA version 3.2.1 (McMullin et al. 2007).

3. ANALYSIS AND RESULTS

A black hole mass has not yet been determined for J17091−3624; a value of 10 $M_\odot$ is assumed throughout this work. Preliminary fits to the HETG spectra of IGR J17091−3624 suggested a relatively high column density, in keeping with values predicted from radio surveys (e.g., $N_{\rm H} = 7.6 \times 10^{21}$ cm^{-2}; Dickey & Lockman 1990). Due to this high column that predominantly affects lower energies, the MEG spectra have comparatively low sensitivity as compared to the HEG, and were therefore excluded.

The limitations of the HEG and our instrumental configuration enforce an effective lower energy bound of 1.3 keV. In the second observation, the instrumental configuration served to enforce an upper limit to the fitting range of 7.6 keV. This limit was adopted for the first observation as well.

3.1. The Spectral Continuum

The HEG spectra were fit with a fiducial spectral model including an effective H column density (*TBabs*), a disk blackbody component, and a power-law component.

The first observation (MJD 55775) is well described by column density of $N_{\rm H} = 9.9 \pm 0.1 \times 10^{21}$ cm^{-2} and a disk blackbody temperature of 1.3 ± 0.1 keV. The resulting fit gave a $\chi^2/\nu = 2657/3156 = 0.84$. This spectrum is dominated by the disk blackbody component, typical of the high soft state of BHB. A power-law continuum component is not statistically required. An unabsorbed flux of $F_{2-10\ {\rm keV}} = 1.5 \pm 0.1 \times 10^{-9}$ erg cm^{-2} s^{-1} was measured.

The second observation (MJD 55841) also had a consistent flux, $F_{2-10\ {\rm keV}} = 1.9 \pm 0.5 \times 10^{-9}$ erg cm^{-2} s^{-1}. Again, the column density was large, at $N_{\rm H} = 1.22 \pm 0.07 \times 10^{22}$ cm^{-2}. A power-law photon index of $\Gamma = 1.7^{+0.07}_{-0.09}$ and a disk blackbody temperature of 2.3 ± 0.3 keV were measured. This disk temperature is high but common in GRS 1915+105 (see, e.g., Vierdayanti et al. 2010). The resulting χ^2/ν was $2754/3414 = 0.81$.

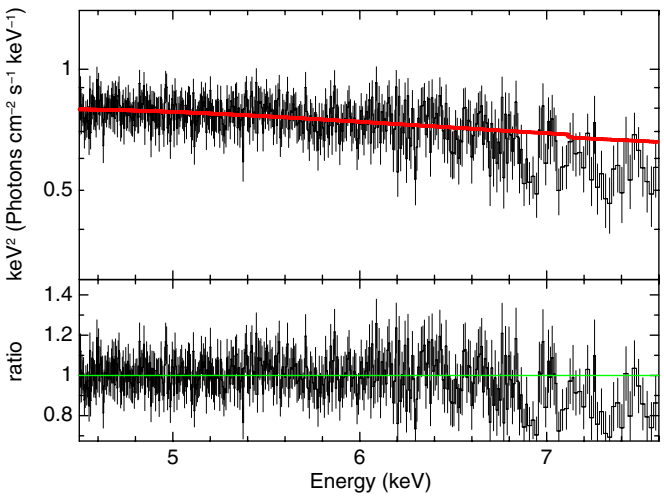

Figure 1. Second *Chandra*/HETG spectrum of IGR J17019−3624 is shown above, fit with a simple disk blackbody plus power-law continuum. The continuum fit excluded the Fe K band to prevent being biased by line features. The line at 6.91 keV is clearly apparent in the data/model ratio. Associating this line with He-like Fe XXV implies an outflow velocity of 9300^{+500}_{-400} km s^{-1}. Weak evidence of a line at 7.32 keV, plausibly associated with Fe XXVI, would imply an even higher outflow velocity. The data were binned for visual clarity.

(A color version of this figure is available in the online journal.)

3.2. The Line Spectra

In the second HEG spectrum, absorption features are noted in the Fe K band (see Figure 1), and these were initially fit with simple Gaussians. The two strongest lines are found at energies of 6.91 ± 0.01 keV and $7.32^{+0.02}_{-0.06}$. Via an *F*-test (see Protassov et al. 2002 for some cautions), these lines are significant at the 99.94% and 99.67% confidence levels, respectively. Dividing the flux normalization of each line by its minus-side error suggests that the feature at 6.91 keV is significant at the 4σ level of confidence, while the 7.32 keV line is marginal at a 2σ confidence level.

We also modeled the second observation continuum with a Comptonization model (*compTT*) instead of the disk blackbody and power law. In general, this gave a reasonable fit at $\chi^2/\nu = 2884/3414 = 0.84$. This model also showed residual absorption features at high energy, which again we modeled with Gaussian functions. Relative to this continuum, the features at 6.91 keV and 7.32 keV are detected at a higher level of significance (6σ).

It is reasonable to associate the line at 6.91 ± 0.01 keV with He-like Fe XXV, which has a rest energy of 6.70 keV (Verner et al. 1996). This translates into a blueshift of 9300^{+500}_{-400} km s^{-1}. This feature clearly signals an extreme disk wind in IGR J17091−3624. Typical velocities in X-ray binaries are <1000 km s^{-1} (Miller et al. 2006a, 2006b). If the feature at $7.32^{+0.02}_{-0.06}$ keV is real and can be associated with H-like Fe XXVI at 6.97 keV, it would correspond to a blueshift of $14{,}600^{+2500}_{-800}$. For additional details, see Table 1. Although less likely, the 6.91 keV line could also be associated with a redshift from the H-like Fe XXVI line. The corresponding inflowing velocity would be 2600 ± 400 km s^{-1}. If this is due to gravitational redshift, the corresponding radius would be $1.7^{+0.3}_{-0.2} \times 10^8$ cm ($60 \pm 10\ R_{\rm Schw}$).

Table 1
Spectral Modeling Parameters of the Second HEG Observation

Parameter	Model 1	Model 2	Model 3	Model 4
	diskbb + po + Gauss + Gauss	(diskbb + po) × Xstar × Xstar	comptt + Gauss + Gauss	(comptt) × Xstar × Xstar
$N_{\rm H}$ (10^{22} cm^{-2})	1.14 ± 0.06	1.13 ± 0.06	$0.475^{+0.017}_{-0.018}$	$0.558^{+0.025}_{-0.028}$
...				
$T_{\rm in}$ (keV)	1.53 ± 0.09	$1.51^{+0.11}_{-0.09}$	...	...
Norm	$13.1^{+3.6}_{-2.5}$	$13.8^{+4.0}_{-1.7}$	...	...
Γ	$1.93^{+0.15}_{-0.16}$	1.91 ± 0.17	...	...
Norm	$0.35^{+0.07}_{-0.08}$	0.34 ± 0.08	...	...
...				
T_0 (keV)	...	...	0.58 ± 0.01	0.59 ± 0.01
kT (keV)	...	...	$10.5^{+30}_{-1.7}$	9.8 ± 0.02
$\tau_{\rm plasma}$	...	...	2.24 ± 0.01	2.28 ± 0.01
Norm	...	...	0.0584 ± 0.0001	$0.062^{+0.002}_{-0.05}$
...				
$E_{\rm Fe\,XXV}$ (keV)	6.91 ± 0.01	...	$6.91^{+0.02}_{-0.01}$	...
FWHM (keV)	$0.091^{+0.022}_{-0.049}$	...	$0.13^{+0.19}_{-0.04}$	...
EW (keV)	$0.021^{+0.005}_{-0.002}$	...	$0.040^{+0.007}_{-0.009}$	...
Norm (10^{-4})	$3.5^{+0.8}_{-0.6}$	...	$6.0^{+1.1}_{-1.3}$	...
v (km s^{-1})	9300^{+500}_{-400}	...	9300^{+400}_{-800}	...
...				
$E_{Fe\,\rm XXVI}$ (keV)	$7.32^{+0.02}_{-0.06}$	...	7.30 ± 0.02	...
FWHM (keV)	$0.081^{+0.079}_{-0.027}$	...	$0.25^{+0.13}_{-0.01}$	...
EW (keV)	$0.032^{+0.018}_{-0.004}$	...	$0.089^{+0.013}_{-0.014}$	...
Norm (10^{-4})	$3.4^{+1.9}_{-0.4}$	...	$11.8^{+1.7}_{-1.6}$	...
v (km s^{-1})	$14{,}600^{+2500}_{-800}$	...	$13{,}800 \pm 800$	...
...				
N (10^{22} cm^{-2})	...	$0.47^{+0.17}_{-0.19}$	...	$0.45^{+0.33}_{-0.17}$
$\log \xi$(erg cm s^{-1})	...	$3.3^{+0.2}_{-0.1}$	...	$3.4^{+0.2}_{-0.1}$
v (km s^{-1})	...	9600^{+400}_{-500}	...	9600 ± 300
...				
N (10^{22} cm^{-2})	...	$1.66^{+1.18}_{-0.83}$	...	$1.97^{+1.26}_{-0.51}$
$\log \xi$(erg cm s^{-1})	...	$3.9^{+0.5}_{-0.3}$	...	$3.7^{+0.3}_{-0.1}$
v (km s^{-1})	...	$15{,}400 \pm 400$	...	$15{,}400^{+400}_{-300}$
...				
χ^2/ν	$2725/3408 = 0.80$	$2731/3408 = 0.80$	$2793/3408 = 0.82$	$2761/3408 = 0.81$

Notes. The line detections using Gaussian functions as well as more self-consistent, photoionization components created with XSTAR, assuming two different continuum models. *TBabs* is applied to all the models and the errors are 1σ confidence level.

The absence of emission lines in the second spectrum of IGR J17091−3624 is notable, but is only suggestive of an equatorial wind. Given that disk winds have only been detected in sources viewed at high inclination angles, and given the similarities between IGR J17091−3624 and GRS 1915+105, it is likely that IGR J17091−3624 is also viewed at a high inclination. However, there is no evidence of eclipses in this source, so inclinations above 70° can be ruled out.

Absorption lines like those detected in the second observation of IGR J17091−3624 are absent in the first observation. Fits to the Fe K band using a local continuum model and narrow Gaussian functions with FWHM values corresponding to those measured in the second observation give 1σ confidence limits of 3 eV or less on lines in the 6.70–7.32 keV band. This is significantly below the equivalent widths measured in the second observation (see Table 1). This may simply be due to a variable absorption geometry in IGR J17091−3624; this has previously been observed in H 1743−322 and GRS 1915+105 (Miller et al. 2006a, 2006b, 2008; Neilsen & Lee 2009).

3.3. Photoionization Modeling

To get a better physical picture of the absorption in the second observation of IGR 17091−3624, we also fit the data with a grid of self-consistent photoionization models created with XSTAR (Kallman & Bautista 2001). The ionizing luminosity for this model was derived from extrapolating the unabsorbed spectrum from the second observation to 0.0136–30 keV, ensuring coverage above 8.8 keV, which is required to ionize Fe XXV. A distance of 8.5 kpc is first assumed to derive this luminosity ($L_{\rm ion} = 3.5 \times 10^{37}$ erg s^{-1}), owing to the location of J17091−3624 within the Galactic bulge. However, Altamirano et al. (2011b) also suggest the possibility that this source could be accreting at high Eddington fractions but further away, and

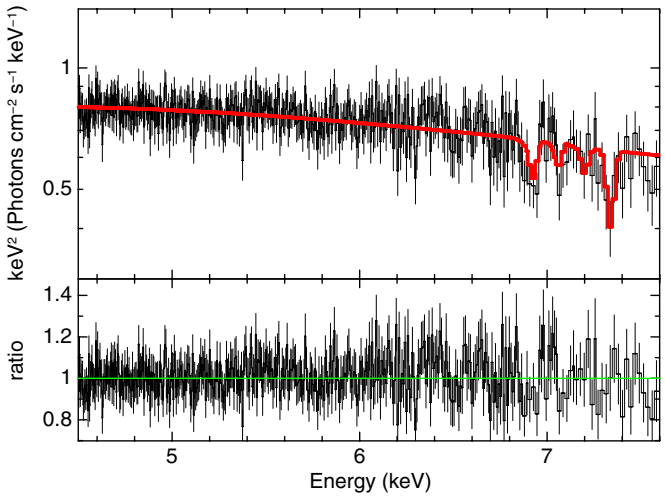

Figure 2. Second *Chandra*/HETG spectrum of IGR J17019−3624 is shown above, fit with a simple disk blackbody plus power-law continuum. A self-consistent photoionization model, generated using XSTAR, was used to model the absorption in the Fe K band. The data were binned for visual clarity.

(A color version of this figure is available in the online journal.)

a distance of 25 kpc was also adopted in a second XSTAR grid ($L_{\rm ion} = 3.5 \times 10^{38}$ erg s^{-1}).

The density of the absorbing material was chosen to be $\log(n) = 12.0$. This is a reasonable assumption based on the modeling of similar X-ray binaries: GX 13+1, $n = 10^{13}$ cm^{-3} (Ueda et al. 2004), GRO J1655−40, $n = 10^{14}$ cm^{-3} (Miller et al. 2008), and H 1743−322, $n = 10^{12}$ cm^{-3} (Miller et al. 2006b). A turbulent velocity of 1000 km s^{-1} was found to provide the best fit after various trials. A covering factor of 0.5 was chosen as the absence of emission lines suggests an equatorial wind. Finally, the Fe abundance was assumed to be twice the solar value after initial fits; this characterizes the Fe K lines but does not predict absorption lines, e.g., Si, that are not observed.

The initial, lower luminosity grid was fit to the data in XSPEC as a multiplicative model; free parameters included the column density, ionization, and velocity shifts of the absorbing gas (see Table 1 and Figure 2). For the disk blackbody and power-law continuum, an ionization parameter of $\log \xi = 3.3^{+0.2}_{-0.1}$ is required, as well as a wind column density of $N = 4.7^{+1.7}_{-1.9} \times 10^{21}$ cm^{-2}. Velocity shifts consistent with simple Gaussian models are found using the XSTAR grid.

To fit the putative higher energy absorption, a second outflow component is required. An additional, lower luminosity XSTAR component is significant at the 3σ level, relative to both continua. The wind column density was higher at $N = 1.7^{+1.2}_{-0.8} \times 10^{22}$ cm^{-2}, and the $\log \xi = 3.9^{+0.5}_{-0.3}$. This system is moving even faster at $15{,}400 \pm 400$ km s^{-1} $= 0.05c$ (see Table 1 and Figure 2).

Repeating this analysis, but utilizing the higher luminosity XSTAR grid, we find that the two components are again required. In fact, the values of the column density, ionization, and velocity shifts are nearly identical and well within 1σ of the previous model.

To derive one estimate to the radius where these winds are launched, we can estimate the radius at which the observed velocity equals the escape velocity. This constrains the radius to be at $r \simeq 2.9 \times 10^9$ cm (970 $R_{\rm Schw}$). Using $\xi = L/(nr^2)$ and $N = nrf$, where f is the one-dimensional filling factor, we can then derive the filling factor and density of the region. Assuming the ionizing luminosity is 3.5×10^{37} erg s^{-1}, the resulting filling factor is $f \simeq 0.0008$, and the density is $n \simeq 2 \times 10^{15}$ cm^{-3}. However, if the luminosity is higher ($L_{\rm ion} = 3.5 \times 10^{38}$ erg s^{-1}), the filling factor decreases to $f \simeq 8 \times 10^{-5}$, and the density increases to $n \simeq 2 \times 10^{16}$ cm^{-3}.

These density estimates are quite high when compared to other X-ray binaries (e.g., Ueda et al. 2004; Miller et al. 2006b, 2008). However, we can invert the previous argument and instead derive the filling factor and radius from an assumed density, i.e., $n = 10^{12}$ cm^{-3}. We find a larger filling factor, ($f \simeq 0.04$), and radius, ($r \simeq 1.3 \times 10^{11}$ cm, 43,300 $R_{\rm Schw}$), if we require a luminosity of 3.5×10^{37} erg s^{-1}. A larger luminosity, i.e., $L_{\rm ion} = 3.5 \times 10^{38}$ erg s^{-1}, reduces the filling factor, ($f \simeq 0.01$), but increases the radius ($r \simeq 3 \times 10^{11}$ cm, 100,000 $R_{\rm Schw}$). At these radii the escape velocity is much lower than the observed velocity.

Finally, we can estimate the mass outflow rate ($\dot{m}_{\rm wind}$) using a modified spherical outflow, which can be approximated as $\dot{m}_{\rm wind} \simeq 1.23 m_p L_{\rm ion} f v \Omega/\xi$. Here, we assume a covering factor $\Omega/4\pi = 0.5$, and an outflowing velocity of $v = 9600$ km s^{-1}. A luminosity of $L_{\rm ion} = 3.5 \times 10^{38}$ erg s^{-1} and filling factor of $f = 8 \times 10^{-5}$ gives a lower limit of $\dot{m}_{\rm wind} \simeq 3.5 \times 10^{16} (10^4/\xi)$ g s^{-1}. However, a much larger outflow rate of $\dot{m}_{\rm wind} \simeq 1.7 \times 10^{18} (10^4/\xi)$ g s^{-1} is found, if we assume $L_{\rm ion} = 3.5 \times 10^{37}$ erg s^{-1} and filling factor of $f = 0.04$.

For comparison, $L = \eta \dot{m}_{\rm acc} c^2$, where η is an efficiency factor typically taken to be 10%. For IGR J17091−3624, $\dot{m}_{\rm acc} = 3.8 \times 10^{17}$ g s^{-1}. Using $\log \xi = 3.3$ from the disk blackbody and power-law model, we find that the observed portion of the outflow is likely to carry away 0.4–20 times the amount of accreted gas. Unless a geometrical consideration serves to bias our estimates, a high fraction of the available gas may not accrete onto the black hole. This trend is not only seen in BHBs but in Seyferts as well. Blustin et al. (2005) note that more than half of their observed Seyferts show $\dot{M}_{\rm out}/\dot{M}_{\rm acc} > 0.3$.

3.4. Radio Non-detections

The EVLA radio observations at 8.4 GHz were made nearly contemporaneously with their X-ray counterparts. Both radio observations were nearly 2 hr in duration. Neither observation detected a source at the location of IGR J17091−3624. The rms noise level for each observation was 0.02 mJy and 0.07 mJy for the two epochs, respectively. The second observation had extended coverage to 4.8 GHz that also had a non-detection. The rms for this frequency was 0.13 mJy. In contrast, IGR J17091−3624 was detected at the 1–2 mJy level during the low/hard state (Rodriguez et al. 2011). This supports prior findings that the radio jet is absent during the periods when winds are seen in BHBs (Miller et al. 2006b, 2008; Neilsen & Lee 2010).

4. DISCUSSION AND CONCLUSIONS

At ionizations above 10^3, radiation pressure is inefficient, and it is not able to drive these winds (e.g., Proga et al. 2000). Thus, although the UV components of disk winds in AGNs are driven at least partially by radiation pressure, the wind in IGR J17091−3624 likely cannot be driven in this way. A thermal wind can arise at radii greater than $0.2R_C$ (Woods et al. 1996), where $R_C = (1.0 \times 10^{10}) \times (M_{\rm BH}/M_\odot)/T_{C8}$, where T_{C8} is the Compton temperature of the gas in units of 10^8 K. The spectrum observed in the second observation gives $R_C \simeq 5 \times 10^{12}$ cm. Therefore, if we assume our conservative estimate of the launching radius, it is possible for IGR J17091−3624 to have a thermally driven wind. However, if the wind originates closer to

the black hole, then it is likely that magnetic processes—either pressure from magnetic viscosity within the disk (e.g., Proga 2003) or magneto-centrifugal acceleration (e.g., Blandford & Payne 1982)—must play a role in launching the wind observed in IGR J17091−3624.

Fast X-ray disk winds are not only seen in BHBs like IGR J17091−3624, but also in AGNs and quasars (e.g., King et al. 2012; Chartas et al. 2002). The fastest UV winds observed in AGNs are pushed to high velocities by radiation pressure. It remains to be seen whether a common driving mechanism works across the black hole mass scale to drive fast, highly ionized X-ray disk winds. Chartas et al. (2002) show that in the quasar APM 08279+5255 there are broad absorption features, which are likely highly relativistic Fe XXV and/or Fe XXVI lines. In these regards, it bears some similarities to the most extreme winds in BHBs.

Observations of BHBs point to an anti-correlation of wind and jet outflows from accretion disks (Miller et al. 2006b, 2008; Blum et al. 2010; Neilsen & Lee 2010). Winds appear to only be detected, or at least are considerably stronger, in soft, disk-dominated states, and absent in hard states where compact, steady jets are ubiquitous (Fender 2006). In H 1743−322, in particular, there is evidence that the absence of winds in hard states is *not* an artifact of high ionization hindering the detection of absorption lines, but instead represents a real change in the column density (and thus the mass outflow rate) in any wind (Blum et al. 2010).

It appears that our coordinated *Chandra* and EVLA observations of IGR J17091−3624 support this anti-correlation. The EVLA observations place very tight limits on the radio flux when the disk wind is detected, orders of magnitude below the level at which IGR J17091−3624 was detected in radio during its low/hard state only a few months prior (Rodriguez et al. 2011).

Neilsen & Lee (2009) suggested that the production of winds may be responsible for quenching jets in GRS 1915+105. It might then be the case that jets should be observed whenever winds are absent. In our first observation of IGR J17091−3624, however, neither a wind nor a jet is detected, with tight limits. Instead, the apparent dichotomy between winds and jets may signal the magnetic field topology in and above the disk is state-dependent. This is broadly consistent with multi-wavelength studies suggesting synchrotron flares above the disk, but only in the hard state (e.g., GX 339−4, XTE J1118+480; Di Matteo et al. 1999; Gandhi et al. 2010). It is interesting to speculate that the magnetic field might be primarily toroidal in the soft state, where a Shakura–Sunyaev disk is dominant, but primarily poloidal in the hard state, when the mass accretion rate is lower (e.g., Beckwith et al. 2008). The type of outflow that is observed may also depend greatly on how much mass is loaded onto magnetic field lines; that could depend on variables including the mass accretion rate through the disk.

We thank the anonymous referee. We thank Michael Nowak for his instrumental help as well. A.L.K. gratefully acknowledges support through the NASA Earth and Space Sciences Fellowship. J.M.M. gratefully acknowledges support through the *Chandra* Guest Observer program. The National Radio Astronomy Observatory is a facility of the National Science Foundation operated under cooperative agreement by Associated Universities, Inc.

REFERENCES

Altamirano, D., Belloni, T., Krimm, H., et al. 2011a, ATel, 3299, 1
Altamirano, D., Belloni, T., Linares, M., et al. 2011b, ApJ, 742, L17
Bautista, M. A., & Kallman, T. R. 2001, ApJS, 134, 139
Beckwith, K., Hawley, J. F., & Krolik, J. H. 2008, ApJ, 678, 1180
Blandford, R. D., & Payne, D. G. 1982, MNRAS, 199, 883
Blum, J. L., Miller, J. M., Cackett, E., et al. 2010, ApJ, 713, 1244
Blustin, A. J., Page, M. J., Fuerst, S. V., Branduardi-Raymont, G., & Ashton, C. E. 2005, A&A, 431, 111
Chartas, G., Brandt, W. N., Gallagher, S. C., & Garmire, G. P. 2002, ApJ, 579, 169
Dickey, J. M., & Lockman, F. J. 1990, ARA&A, 28, 215
Di Matteo, T., Celotti, A., & Fabian, A. C. 1999, MNRAS, 304, 809
Fender, R. 2006, in Jets from X-ray Binaries, ed. W. H. G. Lewin & M. van der Klis (Cambridge: Cambridge Univ. Press), 381
Fruscione, A., McDowell, J. C., Allen, G. E., et al. 2006, Proc. SPIE, 6270, 62701
Gandhi, P., Dhillon, V. S., Durant, M., et al. 2010, MNRAS, 407, 2166
Giroletti, M., & Panessa, F. 2009, ApJ, 706, L260
Jones, S., McHardy, I., Moss, D., et al. 2011, MNRAS, 412, 2641
Kallman, T., & Bautista, M. 2001, ApJS, 133, 221
Kallman, T. R., Bautista, M. A., Goriely, S., et al. 2009, ApJ, 701, 865
Kaspi, S., Brandt, W. N., George, I. M., et al. 2002, ApJ, 574, 643
King, A. L., Miller, J. M., Cackett, E. M., et al. 2011, ApJ, 729, 19
King, A. L., Miller, J. M., & Raymond, J. C. 2012, ApJ, 746, 2
Krimm, H. A., Barthelmy, S. D., Baumgartner, W., et al. 2011, ATel, 3144, 1
Kubota, A., Dotani, T., Cottam, J., et al. 2007, PASJ, 59, 185
Luketic, S., Proga, D., Kallman, T. R., Raymond, J. C., & Miller, J. M. 2010, ApJ, 719, 515
McMullin, J. P., Waters, B., Schiebel, D., Young, W., & Golap, K. 2007, in ASP Conf. Ser. 376, Astronomical Data Analysis Software and Systems XVI, ed. R. A. Shaw, F. Hill, & D. J. Bell (San Francisco, CA: ASP), 127
Miller, J. M., Raymond, J., Fabian, A., et al. 2006a, Nature, 441, 953
Miller, J. M., Raymond, J., Homan, J., et al. 2006b, ApJ, 646, 394
Miller, J. M., Raymond, J., Reynolds, C. S., et al. 2008, ApJ, 680, 1359
Neilsen, J., & Lee, J. C. 2009, Nature, 458, 481
Neilsen, J., & Lee, J. C. 2010, AAS, 42
Proga, D. 2003, ApJ, 585, 406
Proga, D., Stone, J. M., & Kallman, T. R. 2000, ApJ, 543, 686
Protassov, R., van Dyk, D. A., Connors, A., Kashyap, V. L., & Siemiginowska, A. 2002, ApJ, 571, 545
Rodriguez, J., Corbel, S., Caballero, I., et al. 2011, A&A, 533, L4
Tombesi, F., Sambruna, R. M., Reeves, J. N., et al. 2010, ApJ, 719, 700
Ueda, Y., Murakami, H., Yamaoka, K., Dotani, T., & Ebisawa, K. 2004, ApJ, 609, 325
Verner, D. A., Verner, E. M., & Ferland, G. J. 1996, At. Data Nucl. Data Tables, 64, 1
Vierdayanti, K., Mineshige, S., & Ueda, Y. 2010, PASJ, 62, 239
Woods, D. T., Klein, R. I., Castor, J. I., McKee, C. F., & Bell, J. B. 1996, ApJ, 461, 767